Filtration Model for Polydisperse Aerosols in Gas-Solid Flow Using Granule-Resolved Direct Numerical Simulation

R. Kolakaluri, E. Murphy, and S. Subramaniam
Dept. of Mechanical Engineering, Center for Multiphase Flow Research, Iowa State University, Ames, IA 50011

R. C. Brown
Dept. of Mechanical Engineering, Center for Multiphase Flow Research, Iowa State University, Ames, IA 50011

Center for Sustainable Environmental Technologies, Iowa State University, Ames, IA 50011

R. O. Fox
Dept. of Chemical and Biological Engineering, Center for Multiphase Flow Research, Iowa State University, Ames, IA 50011

DOI 10.1002/aic.14901
Published online July 1, 2015 in Wiley Online Library (wileyonlinelibrary.com)

An analytical framework for calculating the filtration efficiency of polydisperse aerosols in a granular bed is developed for cases where inertial impaction and interception are the principal filtration mechanisms. This framework is used to develop a model for the polydisperse single-collector efficiency from monodisperse single-collector efficiency correlations. Conceptually, the polydisperse model is developed by transforming the probability density of particle radius into a probability density of particle Stokes number that is then used to weight the monodisperse single-collector efficiency at a given Stokes number. An extension of this polydisperse filtration concept results in an analytical solution for the axial variation of polydisperse particle flux in a random three-dimensional granule configuration. In order to verify the analytical results for polydisperse particle filtration, a granule-resolved direct numerical simulation approach is coupled with Lagrangian particle tracking to simulate filtration of polydisperse aerosols in a granular bed. © 2015 American Institute of Chemical Engineers *AIChE J*, 61: 3594–3606, 2015
Keywords: granular filtration, direct numerical simulation, analytical model, polydisperse, single-collector efficiency

Introduction

Granular filtration is a process commonly used to remove aerosols from fluid streams. It finds applications in filtration of fly ash from hot gases produced during fast pyrolysis of biomass for bio-oil production,[1,2] water and wastewater treatment,[3] and exhaust gas treatment in thermal power plants. Filtration of particles in these applications is receiving increased attention that is driven by various factors, such as the need for clean coal combustion, treating water pollution, and efforts to reduce risks to human health from exposure to aerosols.

In this study, the word particle is used for the fine particles or aerosols flowing with the fluid and the word granule is used for the bigger particles which form the granular bed through which the fluid flows. The principal mechanisms for particle filtration from fluid streams flowing through a granular bed are inertial impaction, interception, gravitation, and Brownian diffusion.[4] Inertial impaction and interception are significant mechanisms for particle collection in granular filtration for particles with diameters greater than 1 μm and the particles considered in this study fall in this category. Gravitational settling and Brownian diffusion can be neglected for particles with diameters less than 1 mm and particles with diameter greater than 1 μm, respectively.[4] Interial impaction occurs when a particle is so large that it is unable to quickly adjust to the abrupt changes in streamline direction near a granule. Interception occurs when a particle which is following a gas streamline comes within one particle radius of a granule. Granular filtration in the inertial impaction and interception regimes is a strong function of particle inertia that is characterized by the Stokes number $St = |\langle \mathbf{W} \rangle| d_p^2 \rho_p / 9 D_g \mu$.[4–6] The Stokes number is the ratio of the particle momentum response time to a characteristic fluid timescale. The characteristic fluid timescale is taken to be $D_g/2|\langle \mathbf{W} \rangle|$, where $|\langle \mathbf{W} \rangle|$ is the mean slip velocity between fluid and granules and D_g is the granule diameter. Note that it is the mean slip velocity between fluid and *granules* (not particles) that determines the scale of fluid motions. The particle momentum response time is $\tau_p = d_p^2 \rho_p / 18\mu$, where d_p is the diameter of the particle, ρ_p is the density of the particle, and μ is the dynamic viscosity of the fluid.

The aerosols or particles found in the applications mentioned above are generally polydisperse. Furthermore, the process of filtration changes the local size distribution of aerosols at different spatial locations within the granular bed.

Correspondence concerning this article should be addressed to R. Kolakaluri at kravi.aero@gmail.com.
**Present address:* Currently working at 3M Center, St Paul, MN, 55144

Polydispersity implies a range of aerosol Stokes numbers because of the d_p^2 dependence of the particle response time τ_p on diameter. Particles with different Stokes number filter at different rates through a granular bed. In this study, we develop analytical models for polydisperse particle filtration that are valid in both Stokes flow and at moderate mean slip Reynolds number. The mean slip Reynolds number is defined as $Re_m = (1-\epsilon_s)|\langle \mathbf{W} \rangle| D_g \rho_f / \mu$, where ϵ_s is the granule volume fraction, and ρ_f is the fluid density. Note that the mean slip Reynolds number affects the particle Stokes number, which can be written as

$$St = \frac{Re_m}{(1-\epsilon_s)} \left(\frac{d_p}{D_g}\right)^2 \frac{1}{9} \frac{\rho_p}{\rho_f}. \quad (1)$$

The development of analytical polydisperse filtration models for moderate mean slip Reynolds number is one of the principal contributions of this work.

Due to the complex geometry of a granular bed, simple models have been developed to explain filtration. The assumption made in these models is that a granular bed can be represented as a sequence of single collectors, and the filter efficiency of each single collector is called the single-collector efficiency η_s. In this approach,[4] the single-collector efficiency describes the rate of particle collection as the fraction of particles flowing through an area equal to the projected area of the collector in a plane normal to the direction of the flow. The single-collector efficiency η_s for a granular bed is related to the penetration $P = \dot{m}_{out}/\dot{m}_{in}$ by the relation

$$\eta_s = \frac{-2D_g \ln P}{3\epsilon_s L}, \quad (2)$$

where $\dot{m}_{in}$ is the mass of particles injected at the inlet and $\dot{m}_{out}$ is mass of particles exited from the outlet of the granular bed, D_g is the granule diameter, and L denotes the length of the granular bed. Over the past few decades, many researchers have proposed empirical correlations for single-collector efficiency of monodisperse particles based on experimental data.[5,7–9] Correlations are also developed for single-collector efficiency using both numerical and experimental results.[10,11]

For filtration of monodisperse particles in Stokes flow ($Re_m = 0$) through a monodisperse granular bed, the single-collector efficiency η_s depends only on granule volume fraction ϵ_s and particle Stokes number St.[6] For finite mean-slip Reynolds number, the filtration of particles η_s is a function of Stokes number St, granule volume fraction ϵ_s, and the mean slip Reynolds number Re_m. In an attempt to collapse single-collector efficiency data for moderate Reynolds number, the three independent dimensionless groups Re_m, St, and ϵ_s were combined into a single effective Stokes number St_{eff} as given in Eqs. 22 and 23.[5] Most of the correlations for single-collector efficiency found in the granular filtration literature are given as a function of Stokes number St, or a combination of both Stokes number St and mean slip Reynolds number Re_m, or as a function of effective Stokes number St_{eff}. These correlations are for monodisperse particles.

There are very few experimental studies[12,13] on granular filtration of polydisperse aerosols due to difficulties in tracking the filtration rate of each aerosol size class through the granular bed, and also due to the lack of optical access inside the granular bed. While Tien & co-workers[12,13] studied polydispersed aerosol filtration in granular media. However, they did not look at different size distributions of aerosols.

Kim et al.[14] and Kwon et al.[15] analytically calculated the filtration efficiency of a log-normal size distribution of aerosols where Brownian diffusion was considered as the deposition mechanism. Their study does not discuss other size distributions and also the model is limited to Stokes flow. An analytical solution was derived for filtration efficiency of polydisperse aerosols in Stokes flow by Song and Park,[16] where both diffusional and inertial impaction are considered as deposition mechanisms for a log-normal size distribution. All the analytical studies mentioned above are restricted to a log-normal distribution of aerosol diameter. Hence, there is a need for an analytical framework in the inertial impaction regime that is not restricted to a particular size distribution of aerosols, and which is valid in both Stokes flow and at moderate Reynolds number.

The objectives of this work are to develop an analytical framework for polydisperse particle filtration due to inertial impaction and interception that is valid for any size distribution of particles. Another objective is to develop models that are valid in both Stokes flow as well as in moderate Reynolds number flows. In order to verify the analytical model's predictions of polydisperse filtration, a direct numerical simulation (DNS)–Lagrangian particle tracking (LPT) approach is developed to study the filtration of polydisperse particles in a granular bed.

The article is organized as follows. We start with the analytical model development for Stokes flow and moderate Reynolds number flow and the closure models. Following that, the DNS–LPT computational approach that is used to simulate the filtration of particles in a granular bed is described and then we demonstrate convergence of the DNS–LPT approach and comparison of simulation results with experiments. Finally, the analytical predictions for Stokes flow and moderate Reynolds number flow are compared with the DNS–LPT results.

Analytical Model Development

We have seen from various experimental[4,5,8] and numerical studies[6] that the single-collector efficiency for monodisperse particles $\eta_{s,mono}$ is a function of ϵ_s, Re_m, and St, such that $\eta_{s,mono}(\epsilon_s, Re_m, St)$. Therefore, the challenge in developing a model for polydisperse particle filtration is to come up with an expression for $\eta_{s,poly}(\epsilon_s, Re_m, f(r_p))$. The analytical model is first developed for Stokes flow and then extended to moderate Reynolds number flows. It is applied to Stokes flow in a two-dimensional (2-D) ordered array and then to flows at finite Reynolds number in a 3-D assembly of randomly distributed granules that represents a granular bed.

Polydisperse single-collector efficiency in Stokes flow

The principal effect of polydispersity on granular filtration is that the polydisperse single-collector efficiency $\eta_{s,poly}(\epsilon_s, Re_m, f(r_p))$ must account for a range of Stokes number, because the particle-size distribution implies a distribution of Stokes number. For the case of Stokes flow ($Re_m \approx 0$), this dependence can be accounted for by transforming the probability distribution function (PDF) for the particle radius $f(r_p)$ into a PDF for the particle Stokes number $f(St)$ by a simple change of variable

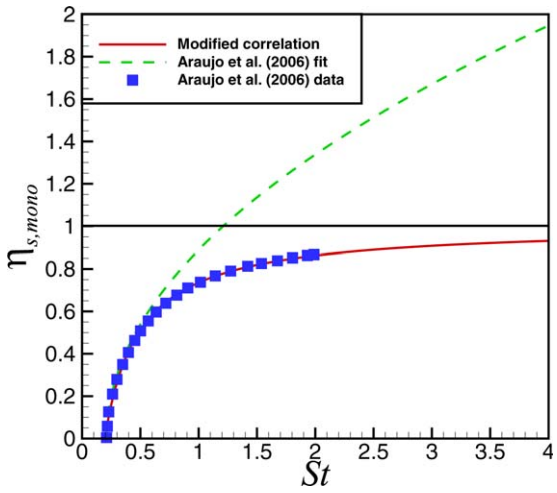

Figure 1. The Araújo et al.[6] correlation and the modified correlation compared with simulation data from Araújo et al.[6] ($\epsilon_s = 0.1$).

[Color figure can be viewed in the online issue, which is available at wileyonlinelibrary.com.]

$$f(\mathrm{St}) = f(r_\mathrm{p})\frac{dr_\mathrm{p}}{dSt} \tag{3}$$

The PDF of particle Stokes number is used to find the polydisperse single-collector efficiency $\eta_{\mathrm{s,poly}}$, which is now expressed as $\eta_{\mathrm{s,poly}}(\epsilon_\mathrm{s}, f(St))$, where the dependence on Re_m can be omitted for Stokes flow. The functional dependence of the monodisperse single-collector efficiency $\eta_{\mathrm{s,mono}}$ on Stokes number can be interpreted as the expected polydisperse single-collector efficiency conditional on a particular Stokes number

$$\eta_{\mathrm{s,mono}}(\epsilon_\mathrm{s}, St) = \langle \eta_{\mathrm{s,poly}} | \epsilon_\mathrm{s}, St \rangle \tag{4}$$

Therefore, the cumulative polydisperse single-collector efficiency is simply

$$\eta^{\mathrm{cum}}_{\mathrm{s,poly}}(\epsilon_\mathrm{s}, St) = \int_{St_\mathrm{c}(\epsilon_\mathrm{s})}^{St} \langle \eta_{\mathrm{s,poly}} | \epsilon_\mathrm{s}, St' \rangle \, f(St') dSt' \tag{5}$$

where St_c is the critical Stokes number above which the filtration of particles starts to take place in the absence of gravity.[6] The effect of interception parameter is not considered in the Araújo et al.[6] study, hence the critical Stokes number St_c is only a function of granule volume fraction ϵ_s. The cumulative polydisperse single-collector efficiency $\eta^{\mathrm{cum}}_{\mathrm{s,poly}}(\epsilon_\mathrm{s}, St)$ represents the filtration efficiency of all particles with $St' < St$. The expected polydisperse single-collector efficiency is $\langle \eta_{\mathrm{s,poly}} \rangle = \eta^{\mathrm{cum}}_{\mathrm{s,poly}}(\infty)$, and is referred to as the total polydisperse efficiency for simplicity. The integral in Eq. 5 is evaluated using fourth-order Runge–Kutta integration.

Results for Stokes flow

Particle filtration in an infinite ordered filter composed of a periodic arrangement of circular obstacles is a classical problem. This approach has been used to describe the porous geometry of fibrous filters[17] and also a homogeneous randomly packed medium.[4] Araújo et al.[6] used the solution of Marshall et al.[17] for flow past a circular obstacle in a square unit cell with periodic boundary conditions imposed on the fluid in both x and y direction to simulate filtration of monodisperse particles. Araújo et al.[6] expressed the single-collector efficiency as a function of particle Stokes number St by

$$\eta_{\mathrm{s,mono}} \propto (St - St_\mathrm{c})^{0.5} \tag{6}$$

The critical Stokes number St_c is shown to vary with granule volume fraction ϵ_s, where $1-\epsilon_\mathrm{s}$ is the unit cell porosity. The correlation given by Araújo et al.[6] exceeds unity for Stokes number greater than 1.2, which is unphysical. In order to remedy this behavior, we propose a modified correlation to Araújo's data for $\eta_{\mathrm{s,mono}}$ for a granule volume fraction ϵ_s of 0.1

$$\eta_{\mathrm{s,mono}} = \frac{(St - St_\mathrm{c})}{(St - St_\mathrm{c}) + a} \tag{7}$$

where $a = 0.31$ and $St_\mathrm{c} = 0.21 (\epsilon_\mathrm{s} = 0.1)$. Figure 1 shows both the modified correlation and original correlation along with the numerical data from Araújo et al.[6] It is observed that the modified correlation fits the data more closely and obeys the correct limiting behavior ($\eta_s \to 1$).

The analytical model prediction (Eqs. 5 and 7) are tested for different size distributions, and compared with LPT results in the latter part of this study. The mean particle radius in this test case is chosen in such a way as to maintain the mean Stokes number ($St(\langle r_\mathrm{p} \rangle) = 0.5$) and particle density ($\rho_\mathrm{p} = 1000$ kg/m^3) close to values found in experiments.[1] The parameters that define the test case are given in Table 1.

The PDFs of particle radius r_p for three size distributions—normal, log-normal, and gamma—that are used to test the cumulative polydisperse single-collector efficiency are shown in Figure 2a. The distributions chosen have analytically integrable forms, however, one of these, the lognormal distribution is often used in the aerosol literature and shown to match with aerosol distributions.[18,19] The corresponding PDF of particle Stokes number obtained using Eq. 3 is shown in Figure 2b. The shape of these distributions affect the cumulative polydisperse single-collector efficiency computed using Eq. 5. Note that the particles in these distributions with $St < St_\mathrm{c}$ do not filter and the critical Stokes number is marked in Figure 2b.

The cumulative polydisperse single-collector efficiency is computed using Eqs. 4 and 5 and the expression for $\eta_{\mathrm{s,mono}}$ (Eq. 7). The cumulative polydisperse single-collector efficiency for the three size distributions is shown in Figure 3. For comparison, the monodisperse single-collector efficiency at the mean particle radius is also shown. The monodisperse single-collector efficiency at the mean particle size is higher than the polydisperse single-collector efficiencies because particles with $St < St_\mathrm{c}$ do not filter out (cf. Eqs. 6 and 7) in all three distributions. The polydisperse single-collector efficiency for the normal distribution is slightly less than the

Table 1. Parameters Corresponding to the Test Case for Polydisperse Filtration in Stokes Flow.

Parameter	Value
Physical	
$\langle r_\mathrm{p} \rangle$	0.22×10^{-3} m
$D_\mathrm{g}(\epsilon_\mathrm{s} = 0.1)$	2×10^{-3}m
Standard deviation SD(r_p)	1.57×10^{-5} m
Nondimensional	
Re_m	0.1
ϵ_s	0.1
$St(\langle r_\mathrm{p} \rangle)$	0.5

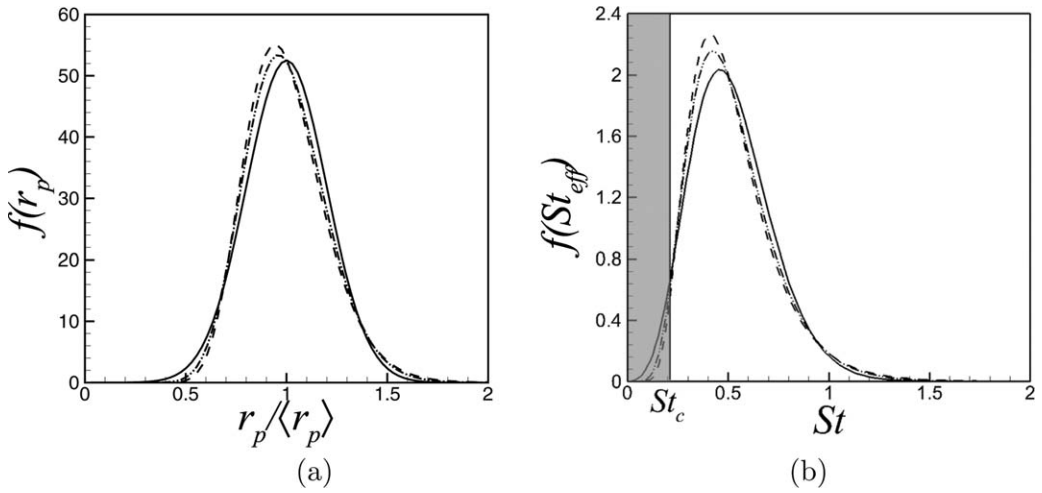

Figure 2. (a) PDF of particle radius for three different distributions with a normalized mean particle radius of 0.11 and normalized standard deviation of 7.85×10^{-3}, both lengths are normalized by D_g. (b) Corresponding PDF's of particle Stokes number for the same distributions with a mean Stokes number of 0.50 based on mean particle radius.(normal —; log-normal - - -; gamma — ·· — ··).

single-collector efficiency of the other two distributions because the peak of the normal distribution is less than that of the log-normal and gamma distributions, whereas the standard deviation is the same for all three distributions (see Figure 2a). The results from this analytical model are compared with 2-D LPT results later in this article.

Polydisperse single-collector efficiency in moderate Reynolds number flow

We now extend the analytical model for polydisperse single-collector efficiency to moderate mean slip Reynolds number. Recall that the experimental data[5] on single-collector efficiency in moderate Reynolds number flow collapses when plotted as a function of the effective Stokes number. The empirical correlation for single-collector efficiency from the experimental data[5] is

$$\eta_{s,\mathrm{mono}}(\epsilon_s, Re_m) = \left(\frac{St_{\mathrm{eff}}^{3.55}}{St_{\mathrm{eff}}^{3.55}+1.67}\right) \tag{8}$$

This motivates the development of a polydisperse single-collector efficiency of the form $\eta_{s,\mathrm{poly}}(\epsilon_s, Re_m, f(St_{\mathrm{eff}}))$. Therefore, the PDF of particle radius is transformed into the PDF of effective Stokes number by a simple change of variables (Eq. 3). The expression for monodisperse single-collector efficiency in moderate Reynolds number flow (given by Eq. 8) is used to obtain the polydisperse filtration efficiency. The cumulative polydisperse single-collector efficiency is

$$\eta_{s,\mathrm{poly}}^{\mathrm{cum}}(\epsilon_s, Re_m, St_{\mathrm{eff}}) = \int_0^{St_{\mathrm{eff}}} \langle \eta_{s,\mathrm{poly}} | St'_{\mathrm{eff}} \rangle f(St'_{\mathrm{eff}}) dSt'_{\mathrm{eff}} \tag{9}$$

Results for moderate Reynolds number flow

The PDFs of particle radius r_p and particle effective Stokes number St_{eff} for three size distributions—normal, log-normal, and gamma—that are used to test the cumulative polydisperse single-collector efficiency are shown in Figures 4a, b. The trends are similar to that observed in the Stokes flow case. The shape of the distributions affect the polydisperse single-collector efficiency. The parameters of the size distributions for the moderate Reynolds number test case are given in Table 2. The two test cases (see Table 3 and 4) chosen are based on experimental data.[5] Test case A with an effective Stokes number $St_{\mathrm{eff}} = 0.72$ falls in the low efficiency region (Figure 9) and test case B with an effective Stokes number $St_{\mathrm{eff}} = 1.12$ falls in the high efficiency region (Figure 9). We also maintained other parameters such as particle density, mean Reynolds number, and granule volume fraction close to experiments.[5]

The cumulative polydisperse single-collector efficiency obtained from all three distributions are shown in Figure 5. For comparison, the monodisperse single-collector efficiency at the mean particle radius is also plotted in Figure 5. In this moderate Reynolds number case with $Re_m = 10$, the total polydisperse single-collector efficiency is higher than the monodisperse value at the mean particle radius because the particles

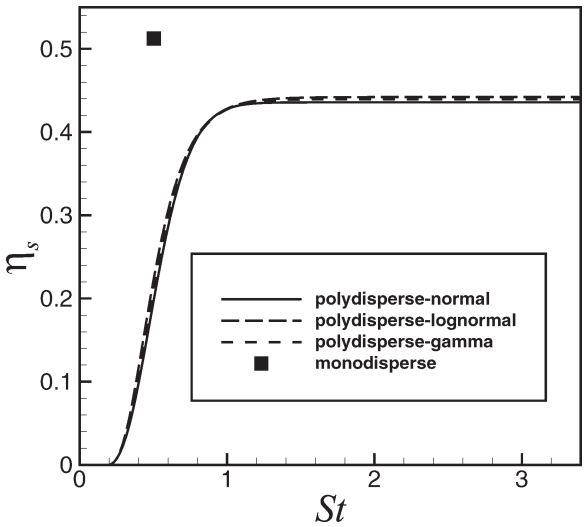

Figure 3. The single-collector efficiency obtained from three different distributions for a normalized standard deviation of 1.52×10^{-2} and a normalized mean particle radius of 0.21 compared with monodisperse single-collector efficiency for the same mean (mean Stokes number = 0.50), both lengths are normalized by D_g.

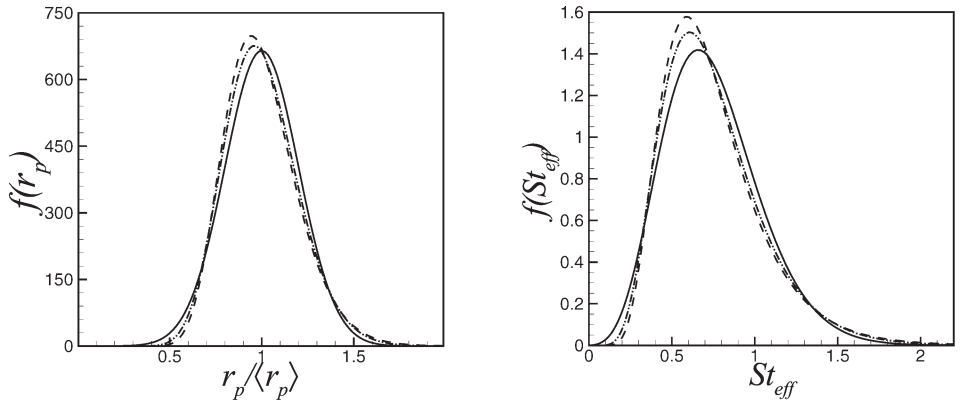

Figure 4. (a) PDF of particle radius for three different distributions with a normalized mean particle radius of 3×10^{-3} and a normalized standard deviation of 6×10^{-4}, both lengths are normalized by D_g. (b) Corresponding PDF's of particle effective Stokes number for the same distributions with a mean effective Stokes number of $St_{eff} = 0.72$ based on normalized mean particle radius, granule volume fraction $\epsilon_s = 0.5$, and mean slip Reynolds number $Re_m = 10$ (normal —; log-normal - - -; gamma — ·· — ··).

with $St_{\text{eff}} > \langle St_{\text{eff}} \rangle$ contribute to this increase. Since the shapes of $f(St_{\text{eff}})$ for $St_{\text{eff}} > \langle St_{\text{eff}} \rangle$ are very similar for all three distributions (see Figure 4b), this increase is very similar for all the three distributions considered.

In this section, we have developed an analytical model for calculating the polydisperse single-collector efficiency for different size distributions of particles in both Stokes and moderate Reynolds number flow. We find that the monodisperse single-collector efficiency at the mean particle radius is not a good estimate of total filtration efficiency since it can over or underpredict the total polydisperse single-collector efficiency depending on the flow conditions. However, the analytical models developed in this section do not provide information regarding the axial variation of particle flux along the granular bed. To find the axial variation of polydisperse particles along the granular bed, we derive an analytical expression for the axial variation of particle flux.

Transport equation for the particle flux

The evolution of number density $n(\mathbf{x}, r, t)$ of particles through the granular bed is governed by Eq. A9. If the sink term due to granular filtration is proportional to the local particle flux at that location, then the axial variation of particle flux in a granular bed can be analytically obtained by solving Eq. 10 with a model for the sink term $S = -\lambda(St_{\text{eff}})\langle V_k|r\rangle n(\mathbf{x}, r, t)$. The resulting number density equation is

$$\frac{\partial n(\mathbf{x}, r, t)}{\partial t} + \frac{\partial}{\partial x_k}(\langle V_k|r\rangle n(\mathbf{x}, r, t)) = -\lambda(St_{\text{eff}})\langle V_k|r\rangle n(\mathbf{x}, r, t) \tag{10}$$

where λ is the filter coefficient. The following expression for the filter coefficient is proposed by Ottavio and Goren[5]

$$\lambda(St_{\text{eff}}) = 3\eta_{s,\text{mono}}(St_{\text{eff}})(1-\varepsilon_s)/2D_g \tag{11}$$

where $\eta_{s,\text{mono}}$ is the monodisperse single-collector efficiency, whose dependence on St_{eff} is given by Eq. 8. At steady state, rewriting Eq. 10 in terms of the particle flux in the granular bed $J_k(\mathbf{x}, r) = \langle V_k|r\rangle n(\mathbf{x}, r)$, results in

$$\frac{\partial}{\partial x_k}(J_k(\mathbf{x}, r)) = -\lambda(St_{\text{eff}})J_k(\mathbf{x}, r) \tag{12}$$

Noting that in granular filtration the particle flux varies only in the axial coordinate ($J(\mathbf{x}, r) = J(x, r)$) because the problem is statistically homogeneous in y and z directions, and integrating Eq. 12 along the length of the granular bed yields the following simple relation

$$\frac{J(x, r)}{J(0, r)} = \exp[-\lambda(St_{\text{eff}})x] \tag{13}$$

The axial variation of particle flux $J(x, r)$ can be written in terms of the particle-size distribution conditional on axial location x, as $J(x, r) = J(x)f(r|x)$, where $J(x)$ is the total particle flux and $f(r|x)$ is the PDF of particle radius conditional on axial location. The total particle flux $J(x)$ at a given axial location x is obtained by integrating over all particle size values

$$J(x) = \int_0^\infty J(x, r)dr = \int_0^\infty J(x)f(r|x)dr \tag{14}$$

The PDF of particle radius is not assumed to be the same at all axial locations, but it changes with x as particles filter through the bed. The particle flux equation (Eq. 13) can be deduced using Eq. 14

$$J(x) = \int_0^\infty J(0, r)\exp[-\lambda(St_{\text{eff}})x]dr \tag{15}$$

Equation 15 can be further simplified, additionally, a change of variables is made from r to St_{eff} to obtain the normalized particle flux

Table 2. Parameters Corresponding to the Experiments for Polydisperse Filtration in Moderate Reynolds Number

Parameter	Value
D_g	2×10^{-3} m; 4×10^{-3} m
$\langle r_p \rangle$	3.0×10^{-7}–2.25×10^{-6} m
$N_R = 2r_p/D_g$	1.5×10^{-4}–2.3×10^{-3}

Table 3. Parameters Corresponding to the Test Cases for Polydisperse Filtration in Moderate Reynolds Number Flow

Parameter	Test Case A	Test Case B
$\langle r_p \rangle$	3.0×10^{-3}	3.75×10^{-3}
$N_R = 2r_p/D_g$	6.0×10^{-3}	7.5×10^{-3}
$\text{SD}(r_p)$	6.0×10^{-4}	7.5×10^{-4}

Table 4. Nondimensional Parameters Corresponding to Experiments and the Test Cases for Polydisperse Filtration in Moderate Reynolds Number Flow

	Experiments	Test Case A	Test Case B
Re_m	10 –1000	10	10
ϵ_s	0.63	0.5	0.5
St	8.6×10^{-4} –0.18	0.05	0.078
St_{eff}	0.15 –2.0	0.72	1.12

$$\frac{J(x)}{J(0)} = \int_0^\infty f(St_{eff}|x=0)\exp[-\lambda(St_{eff})x]dSt_{eff} \qquad (16)$$

The significance of Eq. 16 is that it gives the particle flux $J(x)$ at any location x in terms of the inlet particle flux $J(0)$ and the size distribution $f(r)$. The results of the normalized particle flux obtained from Eq. 16 are compared with DNS–LPT results in the last section. We now briefly describe the DNS–LPT simulations.

DNS of Granular Filtration

In granular filtration, there are two solid phases: one comprises the granules through which the fluid flows, and the other solid phase consists of particles that are suspended in the fluid phase. The 3-D fluid-phase flow fields around the granules are obtained using a granule-resolved DNS methodology called Particle-resolved Uncontaminated-fluid Reconcilable Immersed Boundary Method (PUReIBM; see Figure 6). Note that the fine particles are not resolved because such computations are currently infeasible because of the large diameter ratio between the granules and fine particles that results in a very high number of total number of grid points. If we consider one of the simulation cases in this study, where the number of fine particles is around 1,000,000, and if we consider a coarse resolution of 16 × 16 × 16 grid points to resolve a fine particle, this would result in total number of 4,096,000,000 grid points to resolve the fine particles using PUReIBM DNS.

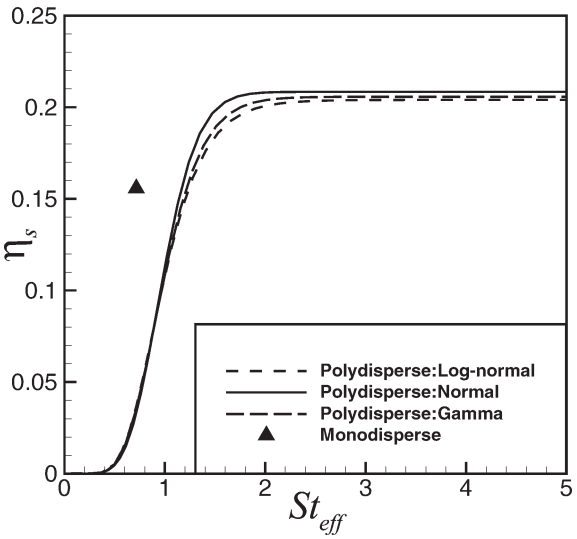

Figure 5. The single-collector efficiency obtained from three different distributions for a normalized standard deviation of 6.0×10^{-4} and a normalized mean particle radius of 3.0×10^{-3} compared with monodisperse single-collector efficiency for the same mean particle radius (mean effective Stokes number $St_{eff} = 0.72$ based on mean particle radius, granule volume fraction $\epsilon_s = 0.5$, and mean slip Reynolds number $Re_m = 10$), both lengths are normalized by D_g.

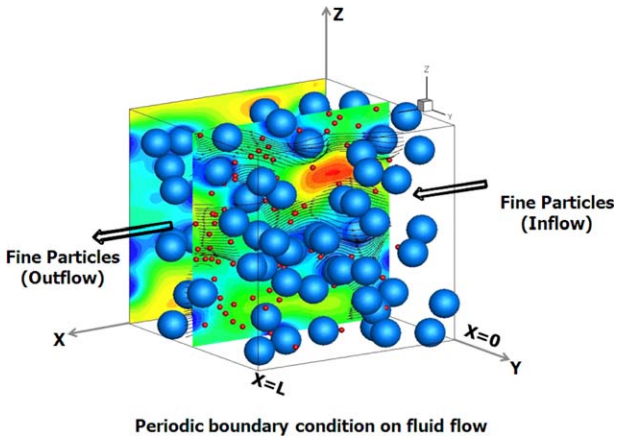

Figure 6. Trapping of particles in a random assembly of granules using DNS–LPT. Contours of the streamwise component of velocity are shown for a granule volume fraction of 0.1 and mean slip Reynolds number of 0.01. The Stokes number of the particles in this simulation is 4×10^{-3}.

In PUReIBM, exact no-slip and no-penetration boundary conditions are imposed at the granule–fluid interface. The governing equations solved in PUReIBM are Eqs. B1 and B2. Details on the PUReIBM solution approach are given in Appendix B. PUReIBM is a numerically convergent and accurate particle-resolved DNS method for fluid-solid flows, and it has been extensively validated in a comprehensive suite of test cases.[20,21] In the DNS–LPT approach developed here, the particles to be filtered are tracked as point particles in a Lagrangian frame as they are carried by the fluid phase through the granular bed.

The dispersed phase consisting of particles is represented in a Lagrangian frame at time t by $\{\mathbf{X}^{(i)}(t), \mathbf{V}^{(i)}(t), d_p^{(i)}(t) i = 1, \ldots\ldots, N_p(t)\}$, where $d_p{}^{(i)}$ denotes the ith particle diameter, $\mathbf{V}^{(i)}(t)$ denotes the ith particle velocity and $\mathbf{X}^{(i)}(t)$ represents its position. The position and velocity of the particles evolve by

$$\frac{d\mathbf{X}^{(i)}(t)}{dt} = \mathbf{V}^{(i)} \qquad (17)$$

and

$$\frac{d\mathbf{V}^{(i)}(t)}{dt} = \frac{\mathbf{f}^{(i)}}{m_p^{(i)}} = \mathbf{A}^{(i)} \qquad (18)$$

where $m_p^{(i)}$ is the mass, and $\mathbf{f}^{(i)}$ and $\mathbf{A}^{(i)}$ are the instantaneous force and acceleration experienced by the ith particle. The particle diameter does not change with time. The instantaneous force is modeled using a drag correlation due to Schiller and Naumann[22]

$$\mathbf{f}^{(i)}(t) = \frac{3\pi\mu|\mathbf{u}(\mathbf{X}^{(i)}(t),t) - \mathbf{V}^{(i)}|d_p^{(i)}(1+0.15Re_p^{0.687})}{C_c} \qquad (19)$$

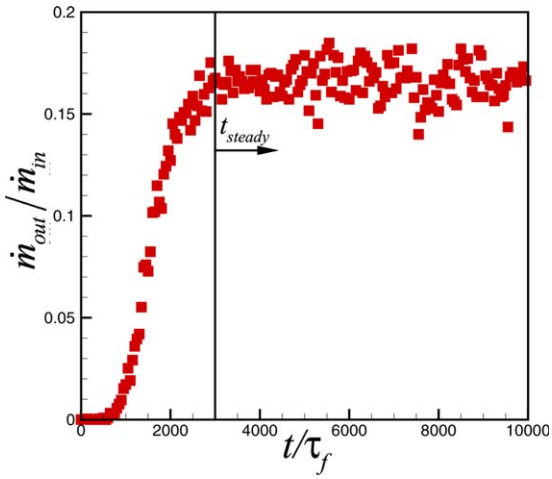

Figure 7. Variation of penetration for a particle Stokes number of $St = 0.10$, granule volume fraction $\epsilon_s = 0.5$, mean-slip Reynolds number $Re_m = 10$ with time t normalized by the fluid time scale τ_f.

[Color figure can be viewed in the online issue, which is available at wileyonlinelibrary.com.]

where C_c is the Cunningham correction factor, $Re_p = \rho_f |\mathbf{u}(\mathbf{X}^{(i)}(t)) - \mathbf{V}^{(i)}| d_p/\mu_f)$ Re_p is the particle Reynolds number based on slip velocity between the fluid and particle (not granule), ρ_f, μ_f, and $\mathbf{u}(\mathbf{X}^{(i)}(t), t)$ are the fluid-phase density, kinematic viscosity, and the velocity of the fluid at the particle location, respectively. The wall effect on the drag force is neglected in this study. Interparticle interactions are neglected consistent with our assumption in the analytical model for particle flux evolution. In this study, the mass loading ($\approx 3\times10^{-2}$) of the dispersed phase negligible, and so momentum exchange between the particles and fluid is neglected (the total particle drag is around $\approx 5\times10^{-2}$ that of the total granule drag for mean slip Reynolds number $Re_m = 10$ and granule volume fraction $\epsilon_s = 0.5$).

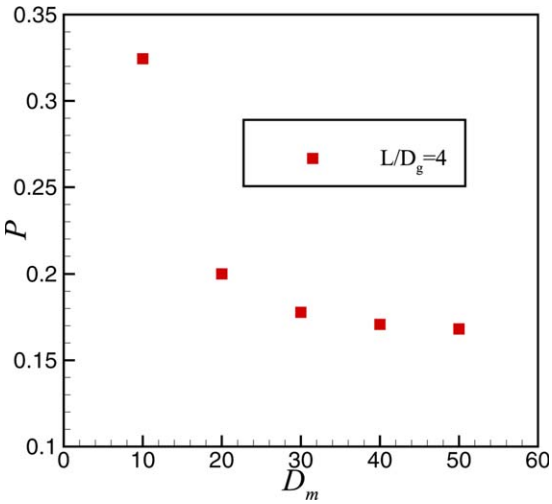

Figure 8. Convergence characteristics of penetration for a particle Stokes number of $St = 0.25$, granule volume fraction $\epsilon_s = 0.4$, mean-slip Reynolds number $Re_m = 20$ with grid resolution D_m for $L/D_g = 4$.

[Color figure can be viewed in the online issue, which is available at wileyonlinelibrary.com.]

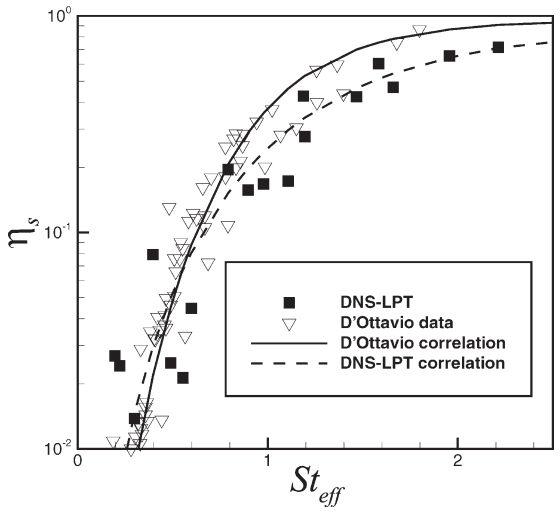

Figure 9. Comparison of single-collector efficiency as a function of effective Stokes number obtained from DNS–LPT simulations with the experimental data[5] and the correlation fitted to those experimental data[5] along with a correlation fitted to DNS–LPT data. Solid squares are simulation results, open gradients are experimental data, the solid line is the D'Ottavio correlation and the dashed line is the correlation fitted to DNS–LPT data.

The fluid velocity at the particle location $\mathbf{u}(\mathbf{X}^{(i)}(t), t)$ is obtained from the fluid velocity at grid nodes. The numerical value of the fluid velocity field $\mathbf{u}(\mathbf{x}, t)$ at the particle location $\mathbf{X}^{(i)}(t)$ is denoted $(\mathbf{u}(\mathbf{X}^{(i)}(t), t))_M$, and is obtained from the representation of $\mathbf{u}$ at M grid nodes through interpolation[23]

$$(\mathbf{u}(\mathbf{X}^{(i)}(t), t))_M = \Im(\mathbf{u}_m, m = 1, ..., M; \mathbf{X}^{(i)}(t)) \qquad (20)$$

where $\mathbf{u}_m$ is the fluid velocity at the m th fluid grid node and $\Im$ is a generic interpolation operation. In this study, we use second-order Lagrange polynomial interpolation.

Simulation approach

Here, we describe how the steady flow field past granules is obtained using the PUReIBM approach. Then the Lagrangian tracking of particles is described. In PUReIBM, the granules are first initialized in a lattice arrangement with a Maxwellian velocity distribution corresponding to a volume fraction of the granules ϵ_s. The granules are then allowed to collide elastically to obtain an equilibrium configuration in the absence of the ambient fluid. A steady flow is then established past the equilibrium particle configuration by imposing a mean pressure gradient that corresponds to a specified mean slip Reynolds number Re_m. The mean pressure gradient evolves in time until it attains the steady value required to drive the desired flow rate. The steady flow fields obtained from PUReIBM are used for Lagrangian tracking of particles. In this work, we simulate steady filtration in flow past fixed granule assemblies, but PUReIBM has been used to simulate moving granules also.[24]

The particles are continuously injected into the computational domain at a specified mass injection rate $\dot{m}_{in}$ (see Fig 6). The particles are assigned the fluid velocity at the initial particle location. The boundary conditions for particles are inflow at $x = 0$, outflow at $x = L$, and periodic in the y and z directions (see Fig 6). A particle is assumed to be trapped by the granular assembly when the distance between the centers of the granule

Table 5. Granular Filtration Parameters for DNS–LPT Validation

Parameters	Values Simulated	Experiments
ϵ_s	0.4, 0.5	0.63
Re_m	10, 20, 30, 50	10 –1000
St	0.05, 0.07, 0.1, 0.25	8.6×10^{-4} –0.18
L/D_g	10	8–50

and the particle is less than $(r_p+D_g/2)$, where r_p is the radius of the particle and D_g is the diameter of the granule. This trapping criterion accounts for both inertial impaction and interception. The particles are removed from the simulation at the outlet plane $x = L$, where L is the length of the computational domain. Figure 6 shows the result of a DNS–LPT simulation. The red spheres are the particles being filtered and the blue spheres are the granules.

DNS–LPT: Numerical Convergence and Comparison with Experiments

Numerical convergence study

Here we establish that the DNS-LPT simulations give numerically converged solutions. We examine the influence of grid resolution $D_m = D_g/\Delta x$ on penetration P, where D_g is the granule diameter, and Δx is the size of each grid cell. The penetration is calculated after the DNS–LPT simulations reach steady state. Figure 7 shows the variation of penetration $P = \dot{m}_{out}/\dot{m}_{in}$ with time, where $\dot{m}_{in}$ is the mass of the particles injected at the inlet and $\dot{m}_{out}$ is the mass of the particles exited from the outlet. The penetration reported in this study is calculated from simulations as

$$P = \frac{\int_{t_{steady}}^{t_{stop}} \dot{m}_{out} dt}{\int_{t_{steady}}^{t_{stop}} \dot{m}_{in} dt} = \frac{m_{out}}{m_{in}} \tag{21}$$

where t_{steady} is the time when the simulation reaches steady state and t_{stop} is the total simulation time. Numerical convergence is shown for a test case with particle Stokes number of 0.25, granule volume fraction 0.4, and a mean slip Reynolds number of 20. Note that L/D_g is a physical parameter in these inflow/outflow simulations, and P decreases with increasing L/D_g. In the test case shown $L/D_g = 4$, but the same convergence holds for $L/D_g = 6, 8, 10$ (results not shown here). Figure 8 shows that the penetration P converges with D_m for $D_m > 30$.

Comparison with experiments

The DNS–LPT computational approach developed to model granular filtration is validated by comparing the penetration P and single-collector efficiency η_s obtained from DNS–LPT with experimental data.[5] A summary of the simulation conditions used to obtain the DNS–LPT data points in Figure 9 is shown in Table 5.

In order to meaningfully compare data from filtration experiments performed with different bed lengths L, it is common practice to compare the single-collector efficiency $(\eta_s = -2D_g \ln P/3\epsilon_s L)$. In Figure 9, we show the variation of single-collector efficiency with effective Stokes number St_{eff}, obtained from both the DNS–LPT and experimental data. The effective Stokes number St_{eff} is defined as

$$St_{eff} = \left[A(\epsilon_s) + 1.14 Re_m^{1/2} (1-\epsilon_s)^{-3/2}\right] \frac{St}{2} \tag{22}$$

$$A(\epsilon_s) = \frac{(6 - 6\epsilon_s^{5/3})}{(6 - 9\epsilon_s^{1/3} + 9\epsilon_s^{5/3} - 6\epsilon_s^{2})} \tag{23}$$

Figure 9 shows a good match of single-collector efficiency obtained from DNS–LPT simulations with experimental data. The scatter in the DNS–LPT data is probably indication of the inadequacy of St_{eff} to collapse η_s data from different (Re_m, ϵ_s) combinations. The solid line in Figure 9 is the correlation (Eq. 8) obtained from experiments[5] and the dashed line in Figure 9 is the new correlation fitted to DNS–LPT data, which reads as

$$\eta_s = \frac{St_{eff}^{2.55}}{3.07 + St_{eff}^{2.55}} \tag{24}$$

Equation 24 will be used for comparison of the analytical particle flux expression with the DNS–LPT date in the last section of this article.

The validation of single-collector efficiency with experimental data shows that the DNS–LPT approach developed in this study gives accurate predictions of granular filtration.

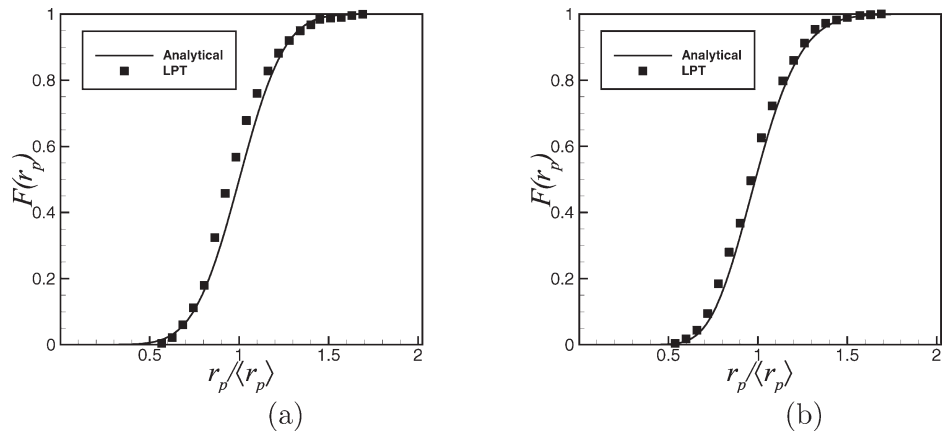

Figure 10. CDF's of particle radius used in the analytical model and LPT simulations: (a) log-normal distribution of normalized particle radius with a mean 0.11 and a normalized standard deviation of 7.85×10^{-3} (mean Stokes number $St = 0.50$ based on mean particle radius), both lengths are normalized by D_g. (b) gamma distribution of normalized particle radius with a mean 0.11 and a normalized standard deviation of 7.85×10^{-3} (mean Stokes number $St = 0.50$ based on mean particle radius), both lengths are normalized by D_g.

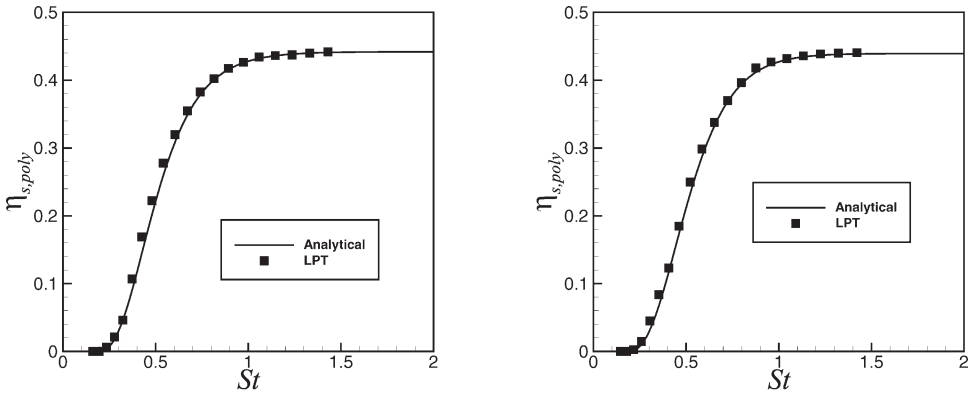

Figure 11. Comparison of cumulative polydisperse single-collector efficiency $\eta_{s,poly}^{cum}$ with Stokes number between the analytical model and LPT simulations: (a) log-normal distribution of normalized particle radius with a mean of 0.11 and a normalized standard deviation of 7.85×10^{-3} (mean Stokes number $St = 0.50$ based on mean particle radius), both lengths are normalized by D_g. (b) gamma distribution of normalized particle radius with a mean of 0.11 and a normalized standard deviation of 7.85×10^{-3} (mean Stokes number $St = 0.50$ based on mean particle radius), both lengths are normalized by D_g.

Comparison of Analytical Model Predictions with the DNS–LPT Results

Polydisperse single-collector efficiency for different particle-size distributions and axial profiles of the particle flux predicted by the polydisperse filtration model are compared with results from the DNS–LPT for both Stokes flow and moderate Reynolds number flow.

Stokes flow

We consider particle filtration in a 2-D unit cell for which Araújo et al.[6] gave a correlation for monodisperse single-collector efficiency (Eq. 6), which is modified for this study (see Eq. 7). We consider a polydisperse distribution of particles injected upstream, and the polydisperse filtration model predicts: (a) the cumulative polydisperse single-collector efficiency as a function of Stokes number and (b) the total polydisperse single-collector efficiency. These are compared with the LPT simulation in flow fields obtained from the improved Kuwabara solution[17] for Stokes flow in a 2-D unit cell. Log-normal and gamma particle-size distributions are considered as test cases. The CDFs of the log-normal and gamma particle-size distributions at the inlet are shown in Figures 10a, b.

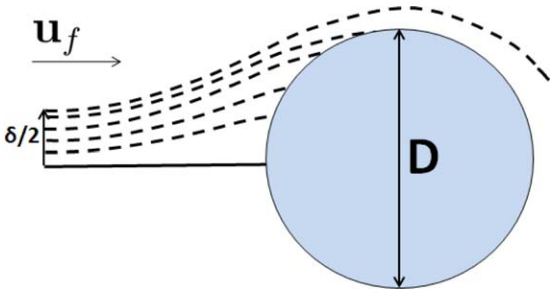

Figure 12. Particle trajectories when released from different positions at the inlet of a periodic unit cell.

[Color figure can be viewed in the online issue, which is available at wileyonlinelibrary.com.]

The cumulative polydisperse single-collector efficiency $\eta_{s,poly}^{cum}$ calculated analytically using Eq. 5 gives a very good match with $\eta_{s,poly}^{cum}$ obtained from LPT results for both log-normal and gamma distributions, as shown in Figures 11a, b. In the LPT simulations, the size distribution is discrete and $\eta_{s,mono}$ is obtained for each discrete particle size, and then $\eta_{s,poly}^{cum}$ is obtained by numerical integration of Eq. 5. A snapshot of the LPT simulation is shown in Figure 12, where $\delta/2$ is the particle Y-coordinate at the inlet of the computational cell, above which the particle will always escape. Note that δ increases with increase in particle size or Stokes number. The

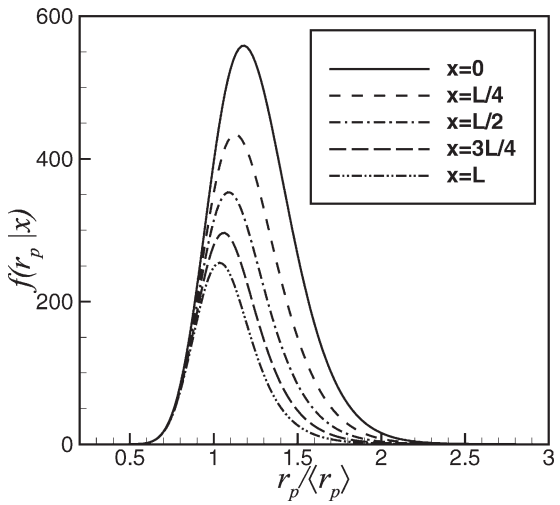

Figure 13. Analytical prediction of particle radius PDF along the granular bed of length L at lengths $x = 0$, $x = L/4$, $x = L/2$, $x = 3L/4$, and $x = L$ for a log-normal distribution of normalized mean particle radius of 3.75×10^{-3} and a normalized standard deviation of 7.5×10^{-4} at the inlet plane (mean effective Stokes number $St_{eff} = 1.12$ based on mean particle radius, granule volume fraction $\epsilon_s = 0.5$ and mean slip Reynolds number $Re_m = 10$), both lengths are normalized by D_g.

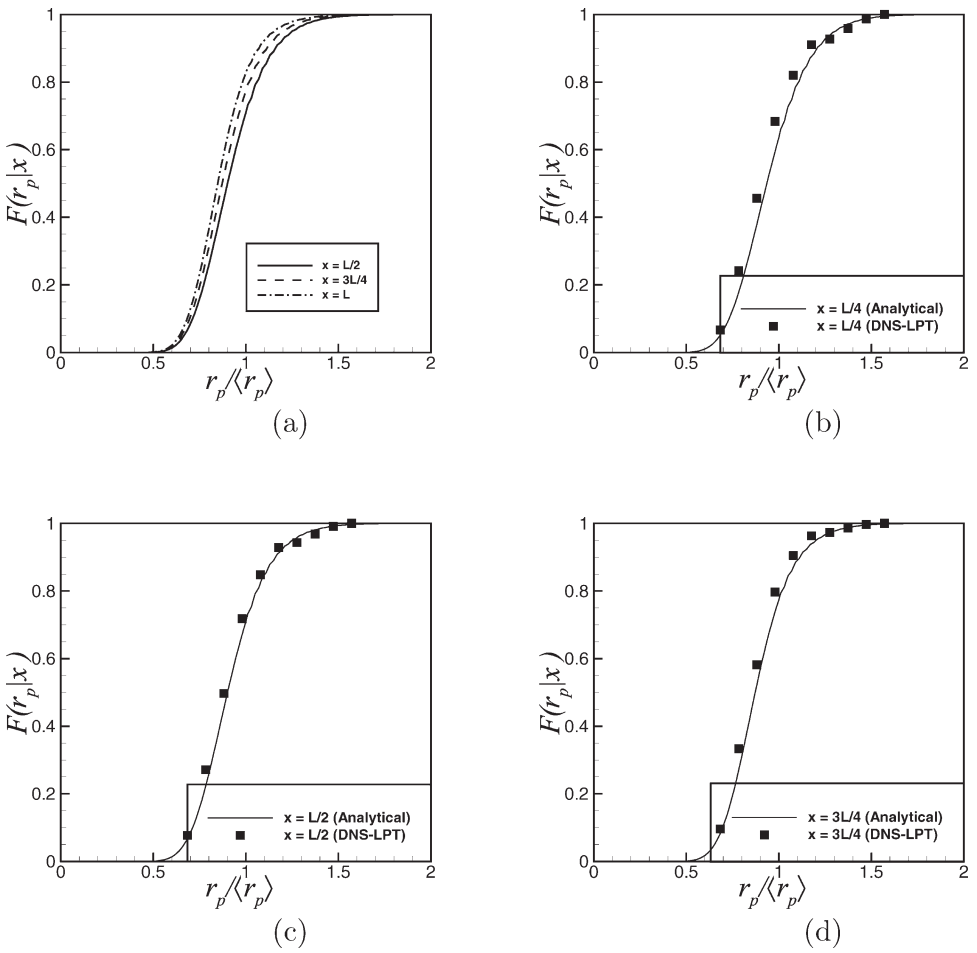

Figure 14. CDF of particle radius along the granular bed of length L, initialized with a log-normal distribution of normalized mean particle radius (by the radius of the granule) of 3.75×10^{-3} and a normalized standard deviation of 7.5×10^{-4} at the inlet plane (mean effective Stokes number $St_{\text{eff}} = 1.12$ based on mean particle radius, granule volume fraction $\epsilon_s = 0.5$, and mean slip Reynolds number $Re_m = 10$), both lengths are normalized by D_g: (a) analytical prediction of particle-size distribution at lengths $L/2$, $3L/4$, and L (b), (c), and (d) comparison of analytical prediction with DNS–LPT simulations at lengths $L/2$, $3L/4$, and L, respectively.

monodisperse single-collector efficiency is $\eta_{s,\text{mono}} = \delta/D$, where D is the diameter of the collector. This simulation approach is similar to that used by Araújo et al.[6] to calculate the single-collector efficiency. These results demonstrate the predictive capability of the model described in the Analytical model development section.

Moderate Reynolds number flow

Particle-size Distribution Along the Granular Bed. We now consider the analytical model's prediction of particle filtration in a 3-D granular bed. In this case, we use an empirical correlation[5] (Eq. 8) for the single-collector efficiency of monodisperse particles. Results obtained from the 3-D analytical model are compared with the DNS-LPT results obtained from the 3-D granular bed for moderate Reynolds number. In the moderate Reynolds number case, the DNS–LPT simulations use the flow fields from PUReIBM.

Recall that our analysis does not assume that the particle-size distribution is constant along the length of granular bed, which is an assumption in most of the analytical models developed in the literature. The expression developed in the Transport Equation for the Particle Flux section (Eq. 16) allows the particle-size distribution to evolve along the length of bed due to variation in the filtration rate of particles of different sizes (Stokes number). In Figure 13, we see how the particle-size distribution varies along the length of the domain.

To understand this analysis further, we modify Eq. 12 as follows to obtain an expression for the evolution of the particle-size distribution

$$\frac{df(r|x)}{dx} = -\frac{1}{J(x)}\frac{dJ(x)}{dx}f(r|x) - \lambda(St_{\text{eff}})f(r|x) \qquad (25)$$

The first term on the right-hand side of Eq. 25 simply rescales the particle-size distribution and the second term changes the shape of the particle-size distribution along the length of the bed. Figure 14a shows the analytical prediction of particle-size distribution at three axial locations in a granular bed, and the comparison of these analytical predictions with the DNS–LPT simulations are shown in Figures 14b, c, and d, respectively. It can be seen in Figure 14 that the particle-size distribution changes along the length of the bed and the analytical model predicts particle-size distributions similar to the DNS–LPT results.

Axial Variation of Particle Flux. Two test cases (test cases A and B in Table 3) are chosen for comparison of the results obtained from the particle flux expression (Eq. 16) with

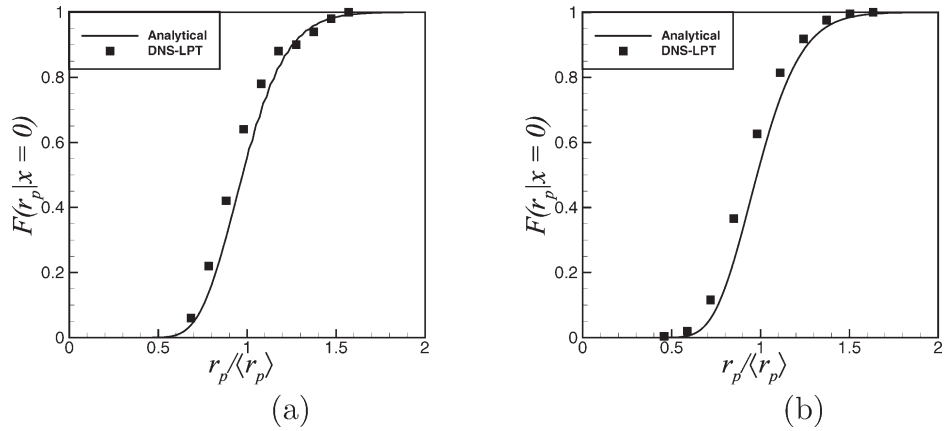

Figure 15. CDF of normalized particle radius at the inlet plane for a log-normal distribution of particles with: (a) normalized mean particle radius of 3.0×10^{-3} and a normalized standard deviation of 6.0×10^{-4} (mean effective Stokes number $St_{eff} = 0.72$ based on mean particle radius, granule volume fraction $\epsilon_s = 0.5$, and mean slip Reynolds number $Re_m = 10$), both lengths are normalized by D_g. (b) normalized mean particle radius of 3.75×10^{-3} and a normalized standard deviation of 7.5×10^{-4} (mean effective Stokes number $St_{eff} = 1.12$ based on mean particle radius, granule volume fraction $\epsilon_s = 0.5$, and mean slip Reynolds number $Re_m = 10$), both lengths are normalized by D_g.

the DNS-LPT results. The CDF of the particle radius for both the test cases are given in Figures 15a, b.

The analytical prediction (see Eq. 16) of steady-state normalized particle flux $J(x)/J(0)$ as a function of axial location x is compared with DNS–LPT results in Figures 16a, b for log-normal particle-size distributions (test cases A and B). The granule solid volume fraction is 0.5 and the mean slip Reynolds number is 10 for these test cases. It should be noted that the error bars in the DNS–LPT simulations are 95% confidence intervals obtained from averaging over five independent simulations corresponding to different granule configurations with the same volume fraction ϵ_s and $g(r)$ (radial distribution function). Figures 16a, b show that the particle flux decays along the axial coordinate due to filtration, and the trend of steady-state normalized particle flux profile predicted by the analytical model is similar to the flux profile of DNS–LPT. It can also be seen in Figures 16a, b that the analytical solution (solid line) overpredicts the decay of particle flux compared to the DNS-LPT results. This overprediction of particle flux decay in both test cases when compared with DNS–LPT data is due to the correlation (Eq. 8) used in the analytical particle flux expression (Eq. 16), which overpredicts the single-collector efficiency when compared with the DNS–LPT (see Figure 9). To confirm this hypothesis, we use the new correlation (Eq. 24) for single-collector efficiency fitted to DNS–LPT. The new correlation (Eq. 24) gives a better fit to DNS–LPT data, as seen in Figure 9. The analytical particle flux expression with Eq. 24 instead of Eq. 8 predicts particle flux profiles (dashed lines in Figures 16a, b) that match the DNS–LPT data. This good agreement between DNS–LPT and the model for axial variation of particle flux lends support to the theoretical formulation in the Transport Equation for the Particle Flux section, allowing prediction of axial flux profiles in granular filtration problems.

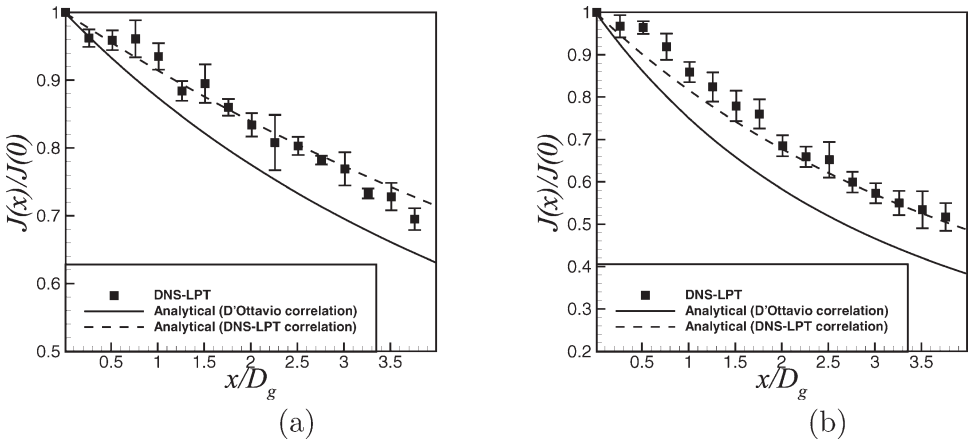

Figure 16. Steady-state normalized particle flux $J(x)/J(0)$ along the flow domain for a log-normal distribution of particles: (a) normalized mean particle radius of 3.0×10^{-3} and a normalized standard deviation of 6.0×10^{-4} (mean effective Stokes number $St_{eff} = 0.72$ based on mean particle radius, granule volume fraction $\epsilon_s = 0.5$, and mean slip Reynolds number $Re_m = 10$), both lengths are normalized by D_g. (b) Normalized mean particle radius 3.75×10^{-3} and a normalized standard deviation of 7.5×10^{-4} (mean effective Stokes number $St_{eff} = 1.12$ based on mean particle radius, granule volume fraction $\epsilon_s = 0.5$, and mean slip Reynolds number $Re_m = 10$), both lengths are normalized by D_g.

Conclusions

We have derived expressions for the cumulative polydisperse single-collector efficiency $\eta_{s,poly}^{cum}(St)$ and total polydisperse single-collector efficiency $\langle \eta_{s,poly} \rangle$ for granular filtration of particles with arbitrary size distributions in Stokes flow and moderate Reynolds number flows. Recognizing the Stokes number as the principal parameter determining filtration due to inertial impaction and interception, we transform the size distribution of particles to a distribution of Stokes number for the Stokes flow case. The expressions are also extended to moderate Reynolds number by converting the size distribution of particles to a distribution of effective Stokes number.

We also derived a transport equation for axial variation of the particle flux for polydisperse particles, which leads to an analytical solution for the size-dependent particle flux as a function of axial location. We developed a DNS–LPT approach for granular filtration of polydisperse particles that is valid for low and moderate Reynolds numbers. The penetration and single-collector efficiency obtained from DNS–LPT results give a good match with existing experimental data.[5] The results obtained from polydisperse analytical model give a very good match with 2-D-LPT and DNS–LPT simulations. The analytical solution for the axial variation of particle flux predicts profiles similar to DNS–LPT results.

Acknowledgments

This work is partially supported by a Department of Energy grant DE-FG36-08-G018205 and NSF grant CMMI-0927660.

Literature Cited

1. El-Hedok IA, Whitmer L, Brown RC. The influence of granular flow rate on the performance of a moving bed granular filter. *Powder Technol*. 2011;214(1):69–76.
2. Ritzert JA, Brown RC, Smeenk J. Filtration efficiency of a moving bed granular filter. *Proceedings of the Science in Thermal and Chemical Biomass Conversion Conference*, Victoria, BC, Canada, August 30–September 2, 2004.
3. Davis ML. *Water and Wastewater Engineering: Design Principles and Practice*. The McGraw-Hill Companies, 2010.
4. Tien C, Ramarao BV. *Granular Filtration of Aerosols and Hydrosols*. Butterworths Series in Chemical Engineering. Elsevier, 2007.
5. D'Ottavio T, Goren SL. Aerosol capture in granular beds in the impaction dominated regime. *Aerosol Sci Technol*. 1982;2(2):91–108.
6. Araújo AD, Andrade JS, Herrmann HJ. Critical role of gravity in filters. *Phys Rev Lett*. 2006;97(13):138001.
7. Thambimuthu KV. Gas filtration in fixed and fluidized beds. Ph.D. thesis. University of Cambridge, Cambridge, 1980.
8. Gal E, Tardos G, Pfeffer R. A study of inertial effects in granular bed filtration. *AIChE J*. 1985;31(7):1093–1104.
9. Jung Y, Walata SA, Tien C. Experimental determination of the initial collection efficiency of granular beds in the inertial-impaction-dominated region. *Aerosol Sci Technol*. 1989;11(2):168–182.
10. Yoshida H, Tien C. A new correlation of the initial collection efficiency of granular aerosol filtration. *AIChE J*. 1985;31(10):1752–1754.
11. Pendse H, Tien C. General correlation of the initial collection efficiency of granular filter beds. *AIChE J*. 1982;28(4):677–686.
12. Jung Y, Tien C. Increase in collector efficiency due to deposition in polydispersed granular filtration—an experimental study. *J Aerosol Sci*. 1992;23(5):525–537.
13. Wu XK, Tien C. Polydispersed aerosol filtration in granular media. *Sep Technol*. 1995;5(2):63–75.
14. Kim HT, Kwon SB, Park YO, Lee KW. Diffusional filtration of polydispersed aerosol particles by fibrous and packed-bed filters. *FiltrationSep*. 2000;37(6):37–42.
15. Kwon SB, Kim HT, Lee KW. Analytic solutions to diffusional deposition of polydisperse aerosols in fibrous filters. *Aerosol Sci Technol*. 2002;36(6):742–747.
16. Song C, Park H. Analytic solutions for filtration of polydisperse aerosols in fibrous filter. *Powder Technol*. 2006;170(2):64–70.
17. Marshall H, Sahraoui M, Kaviany M. An improved analytic solution for analysis of particle trajectories in fibrous, two-dimensional filters. *Phys Fluids*. 1994;6(2):507–520.
18. Friedlander SK. *Smoke, Dust, and Haze: Fundamentals of Aerosol Dynamics*. Oxford University Press, 2000.
19. Hinds WC. *Aerosol Technology: Properties, Behavior, and Measurement of Airborne Particles*. Wiley-Interscience, 1999.
20. Tenneti S, Garg R, Subramaniam S. Drag law for monodisperse gas-solid systems using particle-resolved direct numerical simulation of flow past fixed assemblies of spheres. *Int J Multiphase Flow*. 2011;37(9):1072–1092.
21. Garg R, Tenneti S, Mohd–Yusof J, Subramaniam S. Direct numerical simulation of gas-solids flow based on the immersed boundary method. In: *Computational Gas-Solids Flows and Reacting Systems: Theory, Methods and Practice*. 1st ed. IGI Global, 2010.
22. Schiller L, Naumann AZ. A drag coefficient correlation. *Z Ver Deutsch Ing*. 1935;77:318–320.
23. Garg R, Narayanan C, Lakehal D, Subramaniam S. A numerically convergent Lagrangian-Eulerian simulation method for dispersed two-phase flows. *Int J Multiphase Flow*. 2009;35(4):376–388.
24. Tenneti S, Garg R, Hrenya CM, Fox RO, Subramaniam S. Direct numerical simulation of gas-solid suspensions at moderate Reynolds number: Quantifying the coupling between hydrodynamic forces and particle velocity fluctuations. *Powder Technol*. 2010;20357–69.
25. Williams FA. Spray combustion and atomization. *Phys Fluids*. 1958;1(6):541–545.
26. Subramaniam S. Statistical representation of a spray as a point process. *Phys Fluids*. 2000;12(10):2413–2431.
27. Subramaniam S. Statistical modeling of sprays using the droplet distribution function. *Phys Fluids*. 2001;13(3):624–642.

Appendix A: Derivation of the Number Density Equation

The statistical description at the single particle level is given by the single-particle distribution function $f(\mathbf{x},\mathbf{v},r,t)$ also known as droplet distribution function in spray literature.[25] The $f(\mathbf{x},\mathbf{v},r,t)$ is related to the position, velocity, and radius of the particles by

$$f(\mathbf{x},\mathbf{v},r,t) = \langle f'(\mathbf{x},\mathbf{v},r,t)\rangle = \left\langle \sum_{i=1}^{N_p(t)} f'_i(\mathbf{x},\mathbf{v},r,t) \right\rangle = \left\langle \sum_{i=1}^{N_p(t)} \delta_{\mathbf{X}^{(i)}}\delta_{\mathbf{V}^{(i)}}\delta_{R^{(i)}} \right\rangle \quad \text{(A1)}$$

where $\delta_{\mathbf{X}^{(i)}} = \delta(\mathbf{x}-\mathbf{X}^{(i)}(t))$, $\delta_{\mathbf{V}^{(i)}} = \delta(\mathbf{v}-\mathbf{V}^{(i)}(t))$, $\delta_{R^{(i)}} = \delta(r-R^{(i)}(t))$, p' is the fine-grained density function and f'_i is the fine-grained density function for the ith particle and the expectation in Eq. A1 is over all possible particle configurations and velocities, respectively.[26] The single-particle distribution function $f(\mathbf{x},\mathbf{v},r,t)$ is an unnormalized density function and integrates to the expected total number of particles $\langle N_p(t)\rangle$, such that

$$\langle N_p(t)\rangle = \int_{[\mathbf{x},\mathbf{v},r_+]} f(\mathbf{x},\mathbf{v},r,t)d\mathbf{x}d\mathbf{v}dr \quad \text{(A2)}$$

The evolution equation for $f(\mathbf{x},\mathbf{v},r,t)$[26,27] is

$$\frac{\partial f}{\partial t} + \frac{\partial}{\partial x_k}(v_k f) + \frac{\partial}{\partial v_k}(\langle A_k|\,\mathbf{x},\mathbf{v},r;t\rangle f) = S(\mathbf{x},\mathbf{v},r,t) \quad \text{(A3)}$$

where $S(\mathbf{x},\mathbf{v},r,t)$ is the sink term that arises due to the filtration of particles by granules, and $\langle \mathbf{A}|\,\mathbf{x},\mathbf{v},r;t\rangle$ is the expected acceleration[27] conditional on the location $[\mathbf{x},\mathbf{v},r]$ in phase space. Note that summation is implied over repeated Roman indices. In this study, only the drag force is needed to model the

conditional acceleration term. The particle distribution function can be decomposed as the particle number density $n(\mathbf{x},t)$, and a joint probability density function $f^C_{\mathbf{VR}}(\mathbf{v},r|\,\mathbf{x};t)$[27]

$$f(\mathbf{x},\mathbf{v},r,t) = n(\mathbf{x},t) f^C_{\mathbf{V}R}(\mathbf{v},r|\,\mathbf{x};t) \tag{A4}$$

For the polydisperse size distributions considered in this work, it is convenient to retain size dependence in the number density, as follows

$$n(\mathbf{x},r,t) = \int_{[\mathbf{v}]} f(\mathbf{x},\mathbf{v},r,t)d\mathbf{v} \tag{A5}$$

The decomposition of Eq. A4 in terms of $n(\mathbf{x},r,t)$ becomes

$$f(\mathbf{x},\mathbf{v},r,t) = n(\mathbf{x},r,t) f^C_{\mathbf{V}|R}(\mathbf{v}|r,\mathbf{x};t) \tag{A6}$$

which follows from the following relation

$$f^C_{\mathbf{V}R}(\mathbf{v},r|\,\mathbf{x};t) = f^C_{\mathbf{V}|R}(\mathbf{v}|\,r,\mathbf{x};t) f(r|\,\mathbf{x};t) \tag{A7}$$

and

$$n(\mathbf{x},r,t) = n(\mathbf{x},t) f(r|\,\mathbf{x};t) \tag{A8}$$

where $f(r|\,\mathbf{x};t)$ is the size distribution of particles. The particle position distribution manifests in the particle number density $n(\mathbf{x},r,t)$, which evolves by integrating Eq. A3 over all the velocity space[27] as

$$\frac{\partial n(\mathbf{x},r,t)}{\partial t} + \frac{\partial}{\partial x_k}\left(\langle V_k|r\rangle n(\mathbf{x},r,t)\right) = S(\mathbf{x},r,t) \tag{A9}$$

The evolution equation for number density of monodisperse particles is

$$\frac{\partial n(\mathbf{x},t)}{\partial t} + \frac{\partial}{\partial x_k}\left(\langle V_k\rangle n(\mathbf{x},t)\right) = S(\mathbf{x},t) \tag{A10}$$

Appendix B: Governing Equations Solved in PUReIBM

The mass and momentum equations that are solved at all grid points in PUReIBM are

$$\frac{\partial u_i}{\partial x_i} = 0 \tag{B1}$$

and

$$\rho_f \frac{\partial u_i}{\partial t} + \rho_f S_i = -g_{\mathrm{IBM},i} + \mu \frac{\partial^2 u_i}{\partial x_j \partial x_j} + R_{u,i} \tag{B2}$$

where $g_{\mathrm{IBM},i}$ is the pressure gradient, S_i is the convective term, and $R_{u,i}$ is the immersed boundary force term that accounts for the solid particles in the fluid phase by ensuring no-slip and no-penetration boundary condition at the particle-fluid interface. The thermodynamic density and dynamic viscosity of fluid phase are ρ_f, and μ, respectively. For details about the computation of immersed boundary source term the reader is referred to Garg et al.[21] and Tenneti et al.[20]

In PUReIBM, the governing equations Eqs. B1 and B2 are solved by imposing a periodic boundary condition on fluctuating variables. The velocity field is decomposed into a spatially uniform mean flow and a fluctuating velocity field $\mathbf{u}'$ that is periodic as

$$\mathbf{u}(\mathbf{x},t) = \langle \mathbf{u}\rangle_{\mathcal{V}}(t) + \mathbf{u}'(\mathbf{x},t) \tag{B3}$$

where the volumetric mean velocity is defined as

$$\langle \mathbf{u}\rangle_{\mathcal{V}}(t) = \frac{1}{V}\int_{\mathcal{V}} \mathbf{u}(\mathbf{x},t)d\mathcal{V} \tag{B4}$$

In the same way, the nonlinear term S_i, pressure gradient g_i, and immersed boundary forcing $R_{u,i}$ terms can be decomposed and substituting the decomposed terms in Eqs. B1 and B2 yields the mean momentum conservation equation

$$\rho_f \frac{\partial \langle u_i\rangle_{\mathcal{V}}}{\partial t} = \langle g_i\rangle_{\mathcal{V}} + \langle R_{u,i}\rangle_{\mathcal{V}} \tag{B5}$$

The fluctuating velocity field needs to be divergence free, that is

$$\frac{\partial u_i'}{\partial x_i} = 0 \tag{B6}$$

The conservation equation for the fluctuating momentum can be obtained by subtracting Eq. B5 from Eq. B2, which is

$$\rho_f \frac{\partial u'_i}{\partial t} + \rho_f S'_i = -g'_i + \mu_f \frac{\partial^2 u'_i}{\partial x_j \partial x_j} + R'_{u,i} \tag{B7}$$

Taking divergence of Eq. B7 and using Eq. B6, the modified pressure Poisson equation for the fluctuating pressure gradient can be obtained

$$\frac{\partial g'_{\mathrm{IBM},i}}{\partial x_i} = \frac{\partial R'_{u,i}}{\partial x_i} - \rho_f \frac{\partial S'_i}{\partial x_i} \tag{B8}$$

The equations from Eq. B5 to Eq. B8 are solved to yield the flow field around the granules in PUReIBM.

Manuscript received Sep. 10, 2013, and revision received May 12, 2015.